

A general framework for a joint calibration of VIX and VXX options

Martino Grasselli^{*a,b}, Andrea Mazzoran^{†a}, and Andrea Pallavicini^{‡c,d}

^a*Department of Mathematics, University of Padova, Via Trieste 63 Padova 35121, Italy.*

^b*Devincci Research Center, Léonard de Vinci Pôle Universitaire, 92 916 Paris La Défense, France.*

^c*Department of Mathematics, Imperial College, London SW7 2AZ, United Kingdom.*

^d*Financial Engineering, Intesa Sanpaolo, largo Mattioli 3 Milano 20121, Italy.*

June 15, 2021

Abstract

We analyze the VIX futures market with a focus on the exchange-traded notes written on such contracts, in particular we investigate the VXX notes tracking the short-end part of the futures term structure. Inspired by recent developments in commodity smile modelling, we present a multi-factor stochastic-local volatility model that is able to jointly calibrate plain vanilla options both on VIX futures and VXX notes, thus going beyond the failure of purely stochastic or simply local volatility models. We discuss numerical results on real market data by highlighting the impact of model parameters on implied volatilities.

JEL classification codes: C63, G13.

AMS classification codes: 65C05, 91G20, 91G60.

Keywords: Local volatility, Stochastic volatility, VIX, VIX futures, VXX.

1 Introduction

In recent years, it has become increasingly common to consider volatility as its own asset class. As derivatives on the VIX index, created by the CBOE¹ in 1993, may be inaccessible to non-institutional players, mainly due to the large notional sizes of the contracts as currently designed, some exchange-traded notes (ETN) on the VIX were introduced. In 2009, Barclays launched the first two ETN's on the VIX: VXX² and VXZ. The VXX ETN was the first exchange-traded product (ETP) on VIX futures, issued shortly after the inception of the VIX futures indices. The VXX is a non-securitized debt obligation, similar to a zero-coupon bond, but with a redemption value that depends on the level of the S&P 500 (SPX) VIX Short-Term Futures Total Return index (SPVXSTR). The SPVXSTR

*grassell@math.unipd.it

†andreamazzoran@hotmail.it

‡andrea.pallavicini@intesasanpaolo.com

¹See the white paper of CBOE in 2014 titled *CBOE Volatility Index*, available at <https://www.cboe.com/micro/vix/vixwhite.pdf>.

²See the VXX Prospectus of Barclays available at <https://www.ipathetn.com/US/16/en/instruments.app?searchType=tex>

tracks the performance of a position in the nearest and second-nearest maturing VIX futures contracts, which is rebalanced daily to create a nearly constant 1-month maturity. In other words, VXX mimics the behaviour of the VIX, namely of the 30-day forward-looking volatility, using a replicable strategy based on futures on VIX. Since 2009 then, ETN's on the VIX flourished: there currently exist more than thirty of them, with several billion dollars in market caps and daily volumes (see [Alexander and Korovilas \(2013\)](#) for a comprehensive empirical study on VIX ETN's).

There is a considerable literature for the VIX, and attempts to model VIX can be divided in two strands: on the one hand, the consistent-pricing approach models the joint (risk-neutral) dynamics of the S&P 500 and the VIX with, most often, the aim of pricing derivatives on the two indices in a consistent manner, on the other hand, the stand-alone approach directly models the dynamics of the VIX.

In the former case, we can include the work of [Cont and Kokholm \(2013\)](#) and references therein, while more applications can be found in the work of [Gehricke and Zhang \(2018\)](#), where they propose a consistent framework for S&P 500 (modelled with a Heston-like specification) and the VIX derived from the square root of the variance swap contract. On top of that, they construct the VXX contract from the Prospectus and show that the roll yield of VIX futures drives the difference between the VXX and VIX returns on time series. More recently, in the paper of [Gatheral et al. \(2020\)](#), a joint calibration of SPX and VIX smile has been successfully obtained using the quadratic rough Heston model, while [Guyon \(2020b\)](#) builds up a non-parametric discrete-time model that jointly and exactly calibrates to the prices of SPX options, VIX futures and VIX options. We also mention the work of [Guyon \(2020a\)](#), where the author investigates conditions for the existence of a continuous model on the S&P 500 index (SPX) that calibrates the full surface of SPX and VIX implied volatilities, and the paper of [De Marco and Henry-Labordère \(2015\)](#), where the authors bound VIX options from vanilla options and VIX futures, which leads to a new martingale optimal transport problem that they solve numerically.

In the latter case, the first stand-alone model for the VIX was proposed by Whaley, see [Whaley \(1993\)](#), where he models the spot VIX as a geometric Brownian motion, hence enabling to price options on the VIX in the Black and Scholes framework, but failing to capture the smile effect and the mean-reversion of volatility processes, which is necessary in order to fit the term structure of futures prices ([Schwert \(1990\)](#), [Pagan and Schwert \(1990\)](#) and [Schwert \(2011\)](#)). We cite also the attempt of [Drimus and Farkas \(2013\)](#) based on local volatility. Since then, numerous stand-alone models have been proposed for the VIX. We refer to [Bao et al. \(2012\)](#) and [Lin \(2013\)](#) for a detailed review on that strand of literature.

The literature on VXX is limited. To our knowledge, there are only a few theoretical studies which propose a unified framework for VIX and VXX. Existing studies on the VXX ([Bao et al. \(2012\)](#)) typically model the VXX in a stand-alone manner, which does not take into account the link between VIX and VXX. As a consequence, the loss for VXX when the VIX is in contango cannot be anticipated in such models. In the recent paper of [Gehricke and Zhang \(2020\)](#), they analyze the daily implied volatility curves of the VXX options market alone (where they consider the implied volatility as a function of the moneyness through quadratic polynomial regressions), providing a necessary benchmark for developing a VXX option pricing model. We also mention the work of [Grasselli and Wagalath \(2020\)](#), where the authors link the properties of VXX to those of the VIX in a tractable way. In particular, they quantify the systematic loss observed empirically for VXX when the VIX futures term-structure is in contango and they derive option prices, implied volatilities and skews of VXX from those of VIX in infinitesimal developments.

The affine stochastic volatility model of [Grasselli and Wagalath \(2020\)](#) exploits the FFT methodology in order to price futures and options on VIX, while a Monte Carlo simulation is performed in order to compare the resulting smile on the VXX implied by the calibrated model with the one provided by real market data. The results are not completely satisfactory, which is not surprising, since the VXX can be seen as an exotic path-dependent product on VIX, so that the information regarding the smile on vanillas (on VIX) are well known to be not enough to recover the whole information concerning path dependent products in a purely stochastic volatility model (see for instance [Bergomi \(2015\)](#)).

In the present paper we extend the pure stochastic volatility model for the VIX and we show that a stochastic local-volatility model (SLV) is able to jointly calibrate VIX and VXX options in a consistent manner. The same methodology can be easily extended to other pairs of futures contracts and notes. SLV models are the de-facto industry standard in option pricing since they allow to join the advantages of stochastic volatility models with a good fit of plain options. They were first introduced in [Lipton \(2002\)](#), while a first efficient PDE-based calibration procedure was presented in [Ren et al. \(2007\)](#). In the present paper, since we investigate multi-factor models, we follow the calibration approach of [Guyon and Henry-Labordère \(2012\)](#), which is based on a Monte Carlo simulation. The SLV model we introduce for the VIX futures starts from the work of [Nastasi et al. \(2020\)](#), where the problem of modelling futures smiles for commodity assets in a flexible but parsimonious way is discussed. In particular, here we investigate a multi-factor extension of such model which is tailored to describe VIX futures prices, and to allow a joint calibration of VIX and VXX plain vanilla options.

The key feature of our model is the possibility to decouple the problems of calibrating VIX plain vanilla options, which are recovered by a suitable choice of the local-volatility function, from the more complex task of calibrating the plain vanilla options on the VXX notes. We recall that in our approach the VXX notes are exotic path-dependent product written on VIX futures. We solve the second problem by introducing a local-correlation function between the factors driving the futures prices, and by properly selecting the remaining free dynamics parameters. The calibration of the local correlation function is inspired by the work of [Guyon \(2017\)](#). Quite remarkably, we find that the stochastic component of the volatility is not redundant, namely we need a truly stochastic-local volatility model in order to be able to fit both VIX and VXX markets using real market quotes.

The paper is organized as follows. In Section 2 we give a brief overview of SLV models, highlighting their properties and the main advantages in using these models. In Section 3, we present the general setting of our model. We start from the evolution of a general ETP and their underlying futures contracts, then we describe how to calibrate futures prices and options on futures. In Section 4 we adapt the general framework of the previous section to the case of the VXX ETN strategy. In Section 5 a calibration exercise based on real data along with numerical results and comparisons are presented, involving a joint fit and a parameters sensitivity analysis. In Section 6 we draw some conclusion and remarks.

Needless to say, the views expressed in this paper are those of the authors and do not necessarily represent the views of their institutions.

2 Stochastic local-volatility models

One of the main advantages of using local-volatility models (LV) is their natural modelling of plain-vanilla market volatilities. Indeed, a LV model can be calibrated with extreme

precision to any given set of arbitrage-free European vanilla option prices. LV model were first introduced by Dupire (1994) and Derman and Kani (1994). Although well-accepted, LV models have certain limitations, for example, they generate flattening implied forward volatilities, see Rebonato (1999), that may lead to a mispricing of financial products like forward-starting options.

On the other hand, stochastic volatility (SV) models, like the well known Heston model, see Heston (1993), are considered to be more accurate choices for pricing forward volatility sensitive derivatives, see Gatheral (2011). Although the SV models have desired features for pricing, they often cannot be very well calibrated to a given set of arbitrage-free European vanilla option prices. In particular, the accuracy of the Heston model for pricing short-maturity options in the equity market is typically unsatisfactory.

One possible improvement to the previous issues is considering stochastic local-volatility models (SLV), that take advantages of both LV and SV models properties. SLV models, going back to Jex et al. (1999) and Lipton (2002), are still an intricate task, both from a theoretical as well as a practical point of view. The main advantage of using SLV models is that one can achieve both a good fit to market series data and in principle a perfect calibration to the implied volatility smiles. In such models the discounted price process $(S_t)_{t \geq 0}$ of an asset follows the stochastic differential equation (SDE)

$$dS_t = S_t \ell(t, S_t) \sigma_t dW_t, \quad (2.1)$$

where $(\sigma_t)_{t \geq 0}$ is a process taking positive values, and $\ell(t, K)$ is a sufficiently regular deterministic function, the so-called leverage function, depending on time and on the current value of the underlying asset. The Brownian motion W_t is possibly correlated with the noise driving the process σ . Obviously, SV and LV models are recovered by setting $\ell(t, K) \equiv 1$ or $\sigma \equiv 1$, respectively. At this stage, the stochastic volatility process (which in our specification is given by the product $(\ell \sigma_t)_{t \geq 0}$) can be very general.

The leverage function $\ell(t, K)$ is the crucial part in this model. It allows in principle to perfectly calibrate the market implied volatility surface. In order to achieve this goal, ℓ needs to satisfy the following relation:

$$\ell^2(t, K) = \frac{\eta^2(t, K)}{\mathbb{E}_0[\sigma_t^2 | S_t = K]}, \quad (2.2)$$

where η denotes the local-volatility function, see Dupire (1994). The familiar reader would recognize in Equation (2.2) an application of the Markov-projection procedure, a concept originating from the celebrated Gyöngy Lemma, see Gyöngy (1986), whose idea basically lies in finding a diffusion which “mimics” the fixed-time marginal distributions of an Itô process.

For the derivation of Equation (2.2), we refer to Guyon and Henry-Labordère (2013). Notice that Equation (2.2) is an implicit equation for ℓ as it is needed for the computation of $\mathbb{E}[\sigma_t^2 | S_t = K]$. It is a standard thing in SLV models and this in turn means that the SDE for the price process $(S_t)_{t \geq 0}$ is actually a McKean-Vlasov SDE, since the probability distribution of S_t enters the characteristics of the equation. Existence and uniqueness results for this equation are not obvious in principle, as the coefficients do not typically satisfy standard conditions like for instance Lipschitz continuity with respect to the so-called Wasserstein metric. In fact, deriving the set of stochastic volatility parameters for which SLV models exist uniquely, for a given market implied volatility surface, is a very challenging and still open problem. In the sequel, we will limit to investigate numerically the validity of the assumption just stated in our specific framework.

3 Smile modelling for ETP on futures strategies

We start this section with a wider look to study the volatility smile of a generic ETP based on futures strategies. Then, the results shown in this section will be applied to our specific VXX case in Section 4.

3.1 ETP on futures strategies

We analyze an ETP based on a strategy of N futures contracts F_t^i with maturity dates T_i and $i = 1, \dots, N$. If we assume that the ETP strategy itself is not collateralized and it requires a proportional fee payment ϕ_t , we can write the strategy price process V_t as given by

$$\frac{dV_t}{V_t} = (r_t - \phi_t)dt + \sum_{i=1}^N \omega_t^i \frac{dF_t^i}{F_t^i}, \quad (3.3)$$

where r_t is the risk-free rate. Moreover, we assume that the futures contracts and the ETP are expressed in the same currency as the bank account based on r_t . The processes ω_t^i represent the investment percentage (or weights) in the futures contracts, and they are defined by the ETP term-sheet. Notice that the weights may depend on the whole vector of futures prices. It is straightforward to extend the analysis to more general ETP strategies based on total-return or dividend-paying indices. Moreover, we can introduce securities in foreign currencies as in [Moreni and Pallavicini \(2017\)](#).

We can consider as a first example the family of S&P GSCI commodity indices. Exchange-Traded Commodity (ETC's) tracking these indices are liquid in the market, and they represent an investment in a specific commodity or commodity class. The investment is in the first nearby one-month future, but for the last five days of the contract, where a roll over procedure is implemented to sell the first nearby and to buy the second one. A second example are the volatility-based ETN's VXX and VXXZ. They represent respectively an investment in short-term or in the long-term structure of VIX futures. The investment is in a portfolio of futures mimicking a rolling one-month contract. In Section 4 we will focus on the VXX case.

3.2 Modeling the ETP smile

We wish to jointly model the volatility smile of an ETP and of its underlying futures contracts. Indeed, market quotes for ETP plain-vanilla options can be found on the market. The main problem to solve is the fact that the price process of the ETP strategy is non-Markov, since it depends on the futures contract prices, namely the vector process $[V_t, F_t^1, \dots, F_t^N]$ is Markov.

We start by introducing a generic stochastic volatility dynamics for futures prices under the risk-neutral measure, as given by

$$dF_t^i = \nu_t^i \cdot dW_t, \quad (3.4)$$

where ν_t^i are vector processes in \mathbb{R}^d , possibly depending on the futures prices themselves, and W_t is a d -vector of standard Brownian motions under the risk-neutral measure. The notation $a \cdot b$ refers to the inner product between a and b (vectors or matrices).

In general, we can numerically solve together Equations (3.3) and (3.4) to calculate options prices on the ETP or on the futures contracts. Our aim is at calibrating both the futures and the ETP quoted smile. In the following, we always assume that interest rates and fees are deterministic functions of time, so that we write: $r_t := r(t)$ and $\phi_t := \phi(t)$.

We can simplify the problem by noticing that we need only to know the marginal densities of the futures and ETP prices, so that we can focus our analysis on the Markov projection of the dynamics (3.3) and (3.4). In this way, the model can match the marginal densities of futures prices and ETP prices predicted by the local-volatility model.

Proposition 3.1. (Markov projections) *Given the dynamics (3.4) and (3.3), the Markov projections of the processes F_t^i are given by*

$$d\tilde{F}_t^i = \eta_F^i(t, \tilde{F}_t^i) d\tilde{W}_t^i, \quad \tilde{F}_0^i = F_0^i \quad (3.5)$$

where \tilde{W}_t^i with $i = 1, \dots, N$ are standard Brownian motions under the risk-neutral measure, F_0^i are the futures prices as observed today in the market, and

$$\eta_F^i(t, K) \doteq \sqrt{\mathbb{E}_0[\nu_t^i \cdot \nu_t^i \mid F_t^i = K]}, \quad (3.6)$$

while the Markov projections of the process V_t is given by

$$\frac{d\tilde{V}_t}{\tilde{V}_t} = (r_t - \phi_t) dt + \eta_V(t, \tilde{V}_t) d\tilde{W}_t^0, \quad \tilde{V}_0^i = V_0 \quad (3.7)$$

where \tilde{W}_t^0 is a standard Brownian motion, V_0^i is the ETP price as observed today in the market, and

$$\eta_V(t, K) \doteq \sqrt{\mathbb{E}_0 \left[\sum_{ij=1}^N \hat{\omega}_t^i \nu_t^i \cdot \nu_t^j \hat{\omega}_t^j \mid V_t = K \right]}, \quad (3.8)$$

with the weights $\hat{\omega}_t^i$ given by

$$\hat{\omega}_t^i \doteq \frac{\omega_t^i}{F_t^i}. \quad (3.9)$$

The main ingredient for proving Proposition 3.1 is the Gyöngy Lemma, see Gyöngy (1986), that for the sake of clarity we recall here below.

Lemma 3.1. (Gyöngy Lemma) *Let $X(t)$ be given by*

$$X_t = X_0 + \int_0^t \alpha(s) ds + \int_0^t \beta(s) dW_s, \quad t \geq 0 \quad (3.10)$$

where W is a Brownian motion under some probability measure \mathbb{P} , and α, β are adapted bounded stochastic processes such that (3.10) admits a unique solution. If we define $a(t, x), b(t, x)$ by

$$\begin{aligned} a(t, x) &= \mathbb{E}_0[\alpha(t) \mid X(t) = x] \\ b^2(t, x) &= \mathbb{E}_0[\beta^2(t) \mid X(t) = x], \end{aligned} \quad (3.11)$$

then there exists a filtered probability space $(\tilde{\Omega}, \tilde{\mathcal{F}}, \{\tilde{\mathcal{F}}\}_{t \geq 0}, \tilde{\mathbb{P}})$ where \tilde{W} is a $\tilde{\mathbb{P}}$ -Brownian motion, such that the SDE

$$Y_t = Y_0 + \int_0^t a(s, Y(s)) ds + \int_0^t b(s, Y(s)) d\tilde{W}_s, \quad t \geq 0 \quad (3.12)$$

admits a weak solution that has the same one-dimensional distributions as X . The process Y is called the Markov projection of the process X .

Proof. (Proposition 3.1) Equation (3.5) follows from equation (3.4) and from Lemma 3.1. Dynamics (3.3) can be rewritten as

$$\frac{dV_t}{V_t} = (r_t - \phi_t)dt + \sum_{i=1}^N \omega_t^i \frac{\nu_t^i \cdot dW_t}{F_t^i}, \quad (3.13)$$

and applying Lemma 3.1 we get

$$\eta_V(t, K)^2 = \mathbb{E}_0 \left[\sum_{i,j=1}^N \frac{\omega_t^i \nu_t^i}{F_t^i} \cdot \frac{\nu_t^j \omega_t^j}{F_t^j} \middle| V_t = K \right], \quad (3.14)$$

while the drift part remains unaffected since both r_t and ϕ_t are deterministic functions. The conclusion follows immediately. \square

3.3 Calibration of the local volatility functions

The functions $\eta_F^i(t, K)$ and $\eta_V(t, K)$ are respectively the futures and ETP local-volatility functions. We can calibrate the model on plain-vanilla market quotes using the approach of [Nastasi et al. \(2020\)](#) originally implemented for the commodity market, that is $\eta_F^i(t, K)$ will be calibrated by using options on futures, while $\eta_V(t, K)$ by using options on the ETP strategy. In this approach the Markov projections \tilde{F}_t^i are modelled in term of a common process s_t , which we can identify with the price of a rolling futures contract.

We briefly describe the calibration procedure. We stress that the following assumptions on the dynamics of \tilde{F}_t^i are used only to obtain a simple framework to calibrate the local volatility functions, and they do not pose any constraint on the futures price dynamics F_t^i .

We start by defining the futures local volatilities as given by

$$\eta_F^i(t, K) \doteq \left(K - F_0^i \left(1 - e^{-\int_t^{T_i} a(u) du} \right) \right) \eta(t, k_F^i(t, K)), \quad (3.15)$$

where a is a non-negative function of time, η is a positive and bounded function of time and price, while the effective strike $k_F^i(t, K)$ is given by

$$k_F^i(t, K) \doteq 1 - \left(1 - \frac{K}{F_0^i} \right) e^{\int_t^{T_i} a(u) du}. \quad (3.16)$$

Then, it is possible to show by a straightforward algebra that the above choice allows us to write

$$\tilde{F}_t^i = F_0^i \left(1 - (1 - s_t) e^{-\int_t^{T_i} a(u) du} \right) \quad (3.17)$$

where the driving risk process s_t is modelled by a mean-reverting local-volatility dynamics, namely by

$$ds_t = a(t)(1 - s_t) dt + \eta(t, s_t) s_t dW_t^s, \quad s_0 = 1, \quad (3.18)$$

where W_t^s is a standard Brownian motion under the risk-neutral measure, and we get $W_t^s = \tilde{W}_t^i$ for all the i .

Thus, plain-vanilla options on futures can be calculated as plain-vanilla options on the process s_t , which, in turn, can be easily computed by means of the Dupire equation. More precisely, given the dynamics in Equation (3.18), we have that the normalized call price

$$c(t, k) \doteq \mathbb{E} \left[(s_t - k)^+ \right] \quad (3.19)$$

satisfies the parabolic PDE

$$\partial_t c(t, k) = \left(-a(t) - a(t)(1 - k)\partial_k + \frac{1}{2}k^2\eta^2(t, k)\partial_k^2 \right) c(t, k), \quad (3.20)$$

with boundary conditions

$$c(t, 0) = 1, \quad c(t, \infty) = 0, \quad c(0, k) = (1 - k)^+. \quad (3.21)$$

A more detailed analysis and a proof of this (extended) Dupire equation can be found in [Nastasi et al. \(2020, Proposition 4.1\)](#). Given the prices of options on futures from the market, we can plug their corresponding normalized call prices in Equation (3.20), and then solve it for the function η . Then, we can compute the futures local-volatility function $\eta_F(t, T_i, K)$, thanks to the mapping in Equation (3.15), and eventually recover the prices of options on futures.

There is a vast literature on how to solve Equation (3.20) with the boundary conditions (3.21), here we use an implicit PDE discretization method, as usually done for solving the Dupire equation, see for example [Gatheral \(2011\)](#). We allow a mean-reversion $a(t)$ possibly different from zero when we are calibrating the model to options on futures. On the other hand, options on the ETP spot price can be directly calibrated by a standard local-volatility model, that is without a mean-reversion term. Hence, once $a(t)$ is chosen, we can calibrate to the market $\eta_F^i(t, K)$ and $\eta_V(t, K)$, as previously described.

Thanks to the normalized spot dynamics (3.18), we can price all futures options by evaluating the PDE (3.20), and ETP options as well. In this way we implicitly obtain the marginal probability densities of futures prices and ETP prices.

3.4 Implementing the Markov-projection constraints

We have now to ensure that the two constraints given by the Markov projection (3.6) and (3.8) hold for the futures price dynamics given by Equation (3.4). More precisely, we need to define a suitable dynamics for the processes ν_t^i satisfying the constraints, which in turn enable us to preserve the calibration to plain-vanilla options. A possible strategy is given by selecting the vector processes ν_t^i in the following way.

$$\nu_t^i \doteq \ell_F^i(t, F_t^i) \sqrt{v_t} R_i(t, V_t), \quad (3.22)$$

where the volatility v_t is a scalar positive process to be defined, $\ell_F^i(t, K)$ is the leverage function referred to the futures F_t^i , that can be computed as

$$\ell_F^i(t, K) \doteq \frac{\eta_F^i(t, K)}{\sqrt{\mathbb{E}_0[v_t | F_t^i = K]}}, \quad (3.23)$$

and the d -dimensional vector function $R_i(t, V_t)$ plays the role of local correlation and satisfies the condition $\|R_i(t, V_t)\| = 1$, where $\|\cdot\|$ is the Euclidean norm.

The case of v_t given by a Cox-Ingersoll-Ross process corresponds to a Heston specification for the stochastic volatility. We adopt this choice in the following sections dedicated to the numerical investigations. Another natural candidate for v_t is the Wishart process, which is well known to be able to describe a non trivial dependence among the (positive) diagonal factors, hence going beyond the classic multi-factor Heston model (see e.g. [Da Fonseca et al. \(2007, 2008\)](#)). In Appendix A we provide a choice for the process ν_t^i that exploits the properties of the Wishart specification.

With the definition given by Equation (3.22) for the futures volatilities we obtain that the constraint (3.6) is satisfied by construction, so that the model reprices plain-vanilla options on futures correctly. Yet, the constraint (3.8) is not automatically satisfied. If we substitute the definition of ν_t^i into Equation (3.8), we get

$$\eta_V(t, K) = \sqrt{\sum_{ij=1}^N R_i(t, K) \cdot R_j(t, K) \mathbb{E}_0 \left[v_t \hat{\omega}_t^i \hat{\omega}_t^j \ell_F^i(t, F_t^i) \ell_F^j(t, F_t^j) \mid V_t = K \right]}. \quad (3.24)$$

Thus, in order to complete the calibration of our model, we need to solve the above equation for an (admissible) unknown local function $R_i(t, K)$. We will investigate numerically in practical cases the validity of this assumption.

4 The VXX ETN strategy

We consider the specific case of the VIX futures and the VXX ETN strategy.

4.1 Definition of the ETN strategy

We start by labelling the futures maturity dates $\mathcal{T} := \{T_1, \dots, T_N\}$ from the first date after the observation date t of the price of the ETN strategy. We define for $j = 1, 2, \dots$

$$T^{(0)} := \max \{T \in \mathcal{T} : T < t\}, \quad T^{(j)} := \min \{T \in \mathcal{T} : T > T_{j-1}\}, \quad (4.25)$$

where we assume that at least one maturity date in \mathcal{T} is in the past of t . We name $F_t^{(j)}$ the futures contract with maturity $T^{(j)}$. In particular, we have that $F_t^{(1)}$ is the front contract, and $F_t^{(2)}$ is the second contract.

The VXX is defined as a strategy on the first and second nearby VIX futures as described in [Gehricke and Zhang \(2018\)](#) and given by

$$\frac{dV_t}{V_t} = (r_t - \phi_t)dt + \hat{\omega}_t^{(1)} dF_t^{(1)} + \hat{\omega}_t^{(2)} dF_t^{(2)}, \quad (4.26)$$

where the weights are defined as

$$\hat{\omega}_t^{(1)} \doteq \frac{\alpha(t)}{\alpha(t)F_t^{(1)} + (1 - \alpha(t))F_t^{(2)}}, \quad \hat{\omega}_t^{(2)} \doteq \frac{1 - \alpha(t)}{\alpha(t)F_t^{(1)} + (1 - \alpha(t))F_t^{(2)}}, \quad (4.27)$$

where we define

$$\alpha(t) \doteq \frac{\zeta(T^{(1)}, -1) - \zeta(t, 1)}{\zeta(T^{(1)}, -1) - T^{(0)}}, \quad (4.28)$$

and $\zeta(t, d)$ is a calendar-date shift of d business days.

We notice that the VXX strategy depends on the whole futures term structure, since the futures contracts we identify as front and second contracts change in time. On the other hand, at most two contracts enter the definition at each time, so that the strategy depends only on the correlations between the futures contracts F_t^i and F_t^{i+1} for all $i > 0$.

Remark 4.1. (Definition of the ETP weights.) In [Grasselli and Wagalath \(2020\)](#) a slightly different definition is adopted, by using the year fraction between the second and the first nearby futures as reference time interval, instead of the year fraction between the first nearby and the previous futures contract (without calendar adjustments), leading to

$$\alpha(t) \doteq \frac{T^{(1)} - t}{T^{(2)} - T^{(1)}}. \quad (4.29)$$

4.2 The local correlation

We now implement the modelling framework of the previous sections by using an explicit form for the local-correlation vector. We set the dimension of the Brownian motion vector $d = N$, where N is the number of the futures contracts. Then, we define the local-correlation vector $R_i(t, K)$ as the i -th row of the Cholesky decomposition of the correlation matrix $C(t, K)$ whose elements are given by

$$C_{ij}(t, K) \doteq 1_{\{i=j\}} + 1_{\{i \neq j\}} \rho(t, K), \quad (4.30)$$

where the scalar coefficient $\rho(t, K)$ has values in the range $[-1, 1]$. The above definition satisfies $\|R_i(t, K)\| = 1$ for all i by construction. Moreover, for any $i \neq j$ we get also $R_i(t, K) \cdot R_j(t, K) = \rho(t, K)$.

The particular expression we use for the local-correlation vector leads to simple calibration formulae since it allows us to explicitly calculate the coefficient $\rho(t, K)$ by solving Equation (3.24). In general, a more elaborated structure can be devised if more information on futures correlations are available in the market. For instance, we could consider the VXZ ETN to model more futures contracts, or we can resort to a historical analysis. We leave to a future work such analyses.

We can now calculate the coefficient $\rho(t, K)$ by solving Equation (3.24). We describe in the following proposition the results.

Proposition 4.2. *Given the parametrization of Equation (4.30), the local correlation coefficient $\rho(t, K)$ is given by*

$$\rho(t, K) = \frac{\eta_V^2(t, K) - A^{(1)}(t, K) - A^{(2)}(t, K)}{2A^{(12)}(t, K)}, \quad (4.31)$$

provided that t is not on a futures maturity date, where

$$A^{(1)}(t, K) \doteq \mathbb{E}_0 \left[\left(\hat{\omega}_t^{(1)} \ell_F^{(1)}(t, F_t^{(1)}) \right)^2 v_t \mid V_t = K \right], \quad (4.32)$$

$$A^{(2)}(t, K) \doteq \mathbb{E}_0 \left[\left(\hat{\omega}_t^{(2)} \ell_F^{(2)}(t, F_t^{(2)}) \right)^2 v_t \mid V_t = K \right], \quad (4.33)$$

$$A^{(12)}(t, K) \doteq \mathbb{E}_0 \left[\hat{\omega}_t^{(1)} \hat{\omega}_t^{(2)} \ell_F^{(1)}(t, F_t^{(1)}) \ell_F^{(2)}(t, F_t^{(2)}) v_t \mid V_t = K \right]. \quad (4.34)$$

In the proposition we name $\ell_F^{(1)}(t, K)$ the leverage function of the front futures contract, and accordingly the one of the second contract. The same we do in the proof where we name $\nu^{(1)}$ the volatility of front futures contract. Notice that when t corresponds to a futures maturity date, Equation (4.31) becomes meaningless, because the weights vanish.

Proof. From the definition of the local-volatility $\eta_V(t, K)$ given by Equations (3.8) and (3.24), we get

$$\begin{aligned} \eta_V^2(t, K) &= \mathbb{E}_0 \left[\left(\hat{\omega}_t^{(1)} \right)^2 \nu_t^{(1)} \cdot \nu_t^{(1)} + \left(\hat{\omega}_t^{(2)} \right)^2 \nu_t^{(2)} \cdot \nu_t^{(2)} \mid V_t = K \right] \\ &\quad + 2 \mathbb{E}_0 \left[\hat{\omega}_t^{(1)} \hat{\omega}_t^{(2)} \nu_t^{(1)} \cdot \nu_t^{(2)} \mid V_t = K \right] \\ &= \mathbb{E}_0 \left[\left(\hat{\omega}_t^{(1)} \ell_F^{(1)}(t, F_t^{(1)}) \right)^2 v_t \mid V_t = K \right] \\ &\quad + \mathbb{E}_0 \left[\left(\hat{\omega}_t^{(2)} \ell_F^{(2)}(t, F_t^{(2)}) \right)^2 v_t \mid V_t = K \right] \\ &\quad + 2 \rho(t, K) \mathbb{E}_0 \left[\hat{\omega}_t^{(1)} \hat{\omega}_t^{(2)} \ell_F^{(1)}(t, F_t^{(1)}) \ell_F^{(2)}(t, F_t^{(2)}) v_t \mid V_t = K \right]. \end{aligned} \quad (4.35)$$

Therefore, when t is not on a futures maturity date, we can obtain $\rho(t, K)$ from Equation (4.35) and get the result. \square

We can estimate the conditional expectations by means of the techniques developed in Guyon and Henry-Labordère (2012), namely approximating conditional expectations using smooth integration kernels. Thus, we can evaluate the expectation of a process X_t given a second process Y_t as

$$\mathbb{E}_0[X_t | Y_t = K] \approx \frac{\mathbb{E}_0[X_t \delta^\varepsilon(Y_t - K)]}{\mathbb{E}_0[\delta^\varepsilon(Y_t - K)]}, \quad (4.36)$$

where δ^ε is a suitably defined mollifier of the Dirac delta depending on a smoothing coefficient ε . We can use such approximation within the Monte Carlo simulation for $[V_t, F_t^1, \dots, F_t^N]$ to evaluate the diffusion coefficients of the processes. Alternatively we could use the collocation method developed in Van der Stoep et al. (2014). We stress again that the existence of a solution for Equation (4.31) with the above coefficients is an open question, and, moreover, even if the solution exists, we have to check against market quotes if the chosen parametrization is able to produce a local correlation $\rho(t, K) \in [-1, 1]$ given the plain-vanilla option prices on futures contract and ETP strategy quoted in the market.

Remark 4.2. (Alternative correlation definition) *In order to speed-up the calibration process we can use the following definition of the local-correlation vector exploiting the fact that the VXX ETN depends only on two futures contracts at a time. We set the dimension of the Brownian motion vector $d = 2$, and we define the local-correlation vector $R_i(t, K)$ as given by*

$$R_i(t, K) \doteq 1_{\{i \text{ is odd}\}} R^{(1)}(t, K) + 1_{\{i \text{ is even}\}} R^{(2)}(t, K), \quad (4.37)$$

where the even and odd contributions are defined as

$$R^{(1)}(t, K) \doteq \begin{bmatrix} 1 & 0 \end{bmatrix}, \quad R^{(2)}(t, K) \doteq \begin{bmatrix} \rho(t, K) & \sqrt{1 - \rho^2(t, K)} \end{bmatrix}, \quad (4.38)$$

and the scalar coefficient $\rho(t, K)$ has values in the range $[-1, 1]$. The above definition satisfies $\|R_i(t, K)\| = 1$ and $R_i(t, K) \cdot R_{i+1}(t, K) = \rho(t, K)$ for all i by construction. We can select this alternative definition whenever we are only interested in the price of a contract depending on the front and second futures, as in the VXX case.

4.3 Model specification

We recall the stochastic local-volatility dynamics for the futures prices defined in Section 3, and we select a specific form for the stochastic volatility. From Equations (3.4) and (3.22) we have under the risk-neutral measure

$$dF_t^i = \ell_F^i(t, F_t^i) \sqrt{v_t} R_i(t, V_t) \cdot dW_t, \quad (4.39)$$

where the local-correlation vector $R_i(t, V_t)$ is given by Equations 4.30. We assume that the process v_t follows a one-dimensional CIR process, namely

$$dv_t = \kappa(\theta - v_t) dt + \xi \sqrt{v_t} dZ_t, \quad (4.40)$$

with initial condition $v_0 = \bar{v}$. The Brownian motion Z_t is correlated with the component of the vector W_t . In particular, we select the same correlation for each component, namely $d\langle W_t^i, Z_t \rangle = \rho_v dt$ with $\rho_v \in [-1, 1]$.

VIX Data Set			
T^{VIX}	$F_0(T)$	# options	K (min – max)
T_1 : November 20, 2019	14.60	40	10 – 80
T_2 : December 18, 2019	16.15	40	10 – 80
T_3 : January 22, 2020	17.45	35	10 – 80
T_4 : February 19, 2020	18.15	35	10 – 80

Table 1: VIX futures call options data set as on T_0 : November 7, 2019.

VXX Data Set		
T^{VXX}	# options	K (min – max)
T_1 : November 20, 2019	65	8 – 60
T_2 : December 18, 2019	59	2 – 60
T_3 : January 22, 2020	53	10 – 90

Table 2: VXX call options data set as on T_0 : November 7, 2019. Spot price: $V_0 = 19.22$.

In the above equation the positive constants κ , θ and ξ are respectively the speed of the mean-reversion of the variance, the long-run average variance, and the volatility-of-volatility parameter. Our one-factor specification for the stochastic volatility will turn out to be enough for our purposes. In fact, the apparently more general multifactor choice does not lead to better results in the quality of the fit, up to our numerical experiences.

Finally, we assume also that the mean reversion $a(t)$ is independent of time to reduce the number of free parameters. Thus, we can collect all the parameters of our model not fixed by the calibration procedure in the following vector

$$\Theta := \{a, \bar{v}, \kappa, \theta, \xi, \rho_v\}. \quad (4.41)$$

These parameters can be fine-tuned so that Equation (4.31) leads to a local-correlation coefficient in the valid range $[-1, 1]$. We will see in the next section how to achieve this goal.

5 Numerical illustration on a real data set

In this section we perform a numerical exercise, based on real data quoted by the market for options on the VIX futures and the VXX ETN strategy, where we provide a set of admissible parameters, that is leading to an admissible local correlation vector in Equation (4.31) satisfying $\rho(t, K) \in [-1, 1]$. In this way we build up a coherent framework that correctly reprices plain vanilla options on futures contract and VXX strategy quoted in the market. We stress that the set of parameters we are going to find does not necessarily represent the optimal choice, namely we are just providing an admissible framework, not a full calibration. We leave for future research the complete exploration of this issue.

5.1 VIX and VXX data sets

We test our model against a set of three maturities for VXX call options with a corresponding set of four maturities for VIX futures call options. All data are observed on the market on November 7, 2019. Table 1 (resp. Table 2) describes the features of the VIX (resp. VXX) options data set. In the tables we list also the different maturities of VIX and

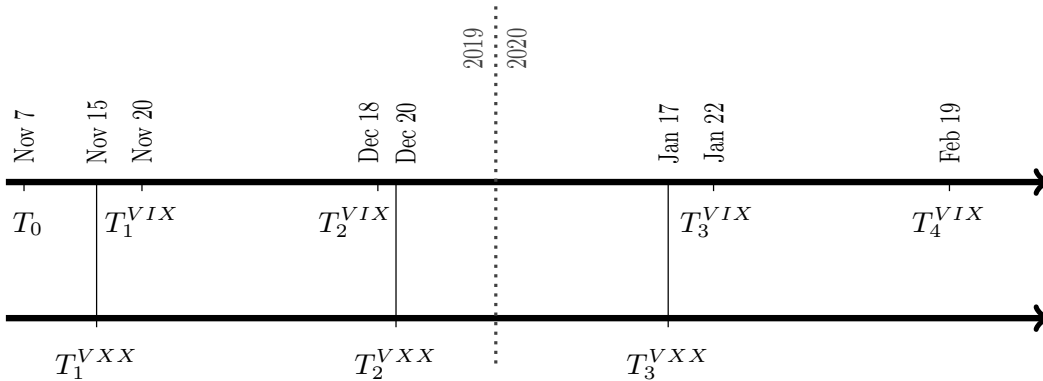


Figure 1: Term structure of VIX and VXX option maturities starting from November 7, 2019.

VXX options involved in the numerical exercise, and the values of VIX futures and VXX spot price, as observed in the market. Market data quotes are shown in the calibration section.

5.2 Parameter sensitivities

We now perform a sensitivity analysis that will highlight the impact of the model parameters on the VXX smiles. The aim of this analysis is to find a range of parameters that guarantees a good fit to the VXX market smile, while maintaining the fit on the VIX market smile. Then we test if these parameters generate a local correlation $\rho(t, K) \in [-1, 1]$, by solving Equation (4.31). More precisely, we let each parameter vary while keeping the others frozen. In this way, we can check the overall impact of each parameter on the shape of the VXX smile. This will give us an insight on the set of reasonable parameters that can generate a good fit, provided that the local correlation in Equation (4.31) is admissible. The analysis is performed by fixing the correlation $\rho = 0.85$.

We shall investigate the impact of the mean-reversion speed a and the volatility-of-volatility ξ . We omit an explicit analysis of the impact of the other parameters \bar{v} , κ , θ and ρ^v , since it turns out empirically that they do not play an important role in the smile modelling. We set in the following $\rho^v = 0.75$, and we choose the remaining three parameters so that the Feller condition holds. In particular, we choose $\kappa = 2.5$, $\theta = 2.5$, $\bar{v} = 1$.

We start by the impact of the mean-reversion a . We perform the simulations with volatility-of-volatility $\xi = 1.1$, while the mean-reversion speed can range from 0 to 8. In Figure 2 we present the results. We get that the higher the mean-reversion, the lower the smile. Thus, in order reproduce the market ATM implied volatility level for the VXX smile we need a high mean-reversion speed, the best match being $a = 7.5$, in particular if we look near the at-the-money level of the first maturity. The (high) value for the mean-reversion speed could seem misconceiving. However, we should keep in mind that we are jointly modelling two markets, the VIX and VXX option books, that display different peculiarities, therefore a somehow non standard level for the mean reversion seems a reasonable price to pay in order to reach our goal.

Then, we consider the impact of the volatility-of-volatility ξ . We perform the simulations with mean-reversion speed $a = 7.5$, while the volatility of volatility can range from 0.1 to 1.3. In Figure 3 we present the results. We observe a relevant impact on the left wing of the smile. The best match seems to be for $\xi = 1.1$, in particular if we look near

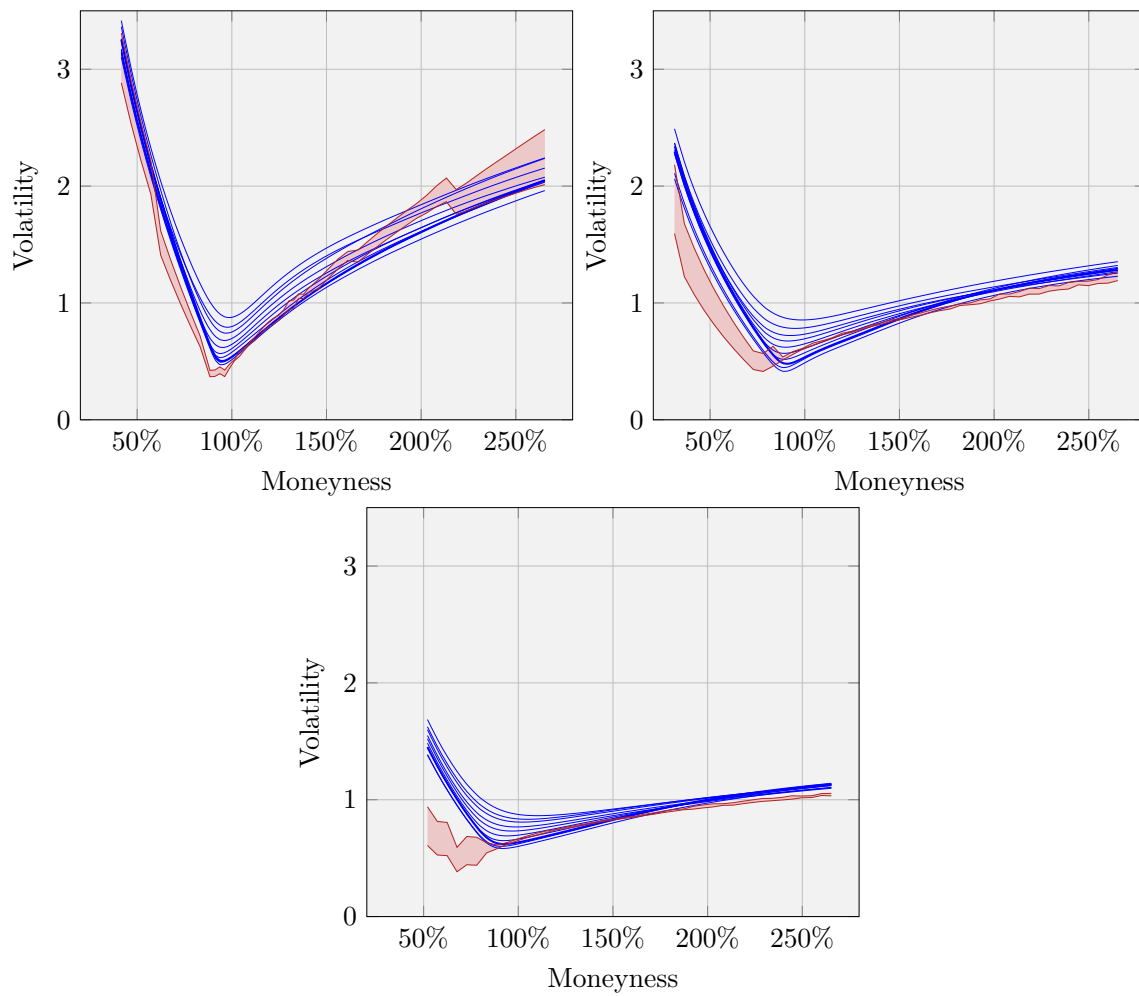


Figure 2: Impact on the VXX smile of the mean-reversion speed. Market bid-ask quotes span the red shaded area, while model implied volatilities are the blue solid lines with mean-reversion speed ranging from 0 to 8. The thick blue line is $a = 7.5$.

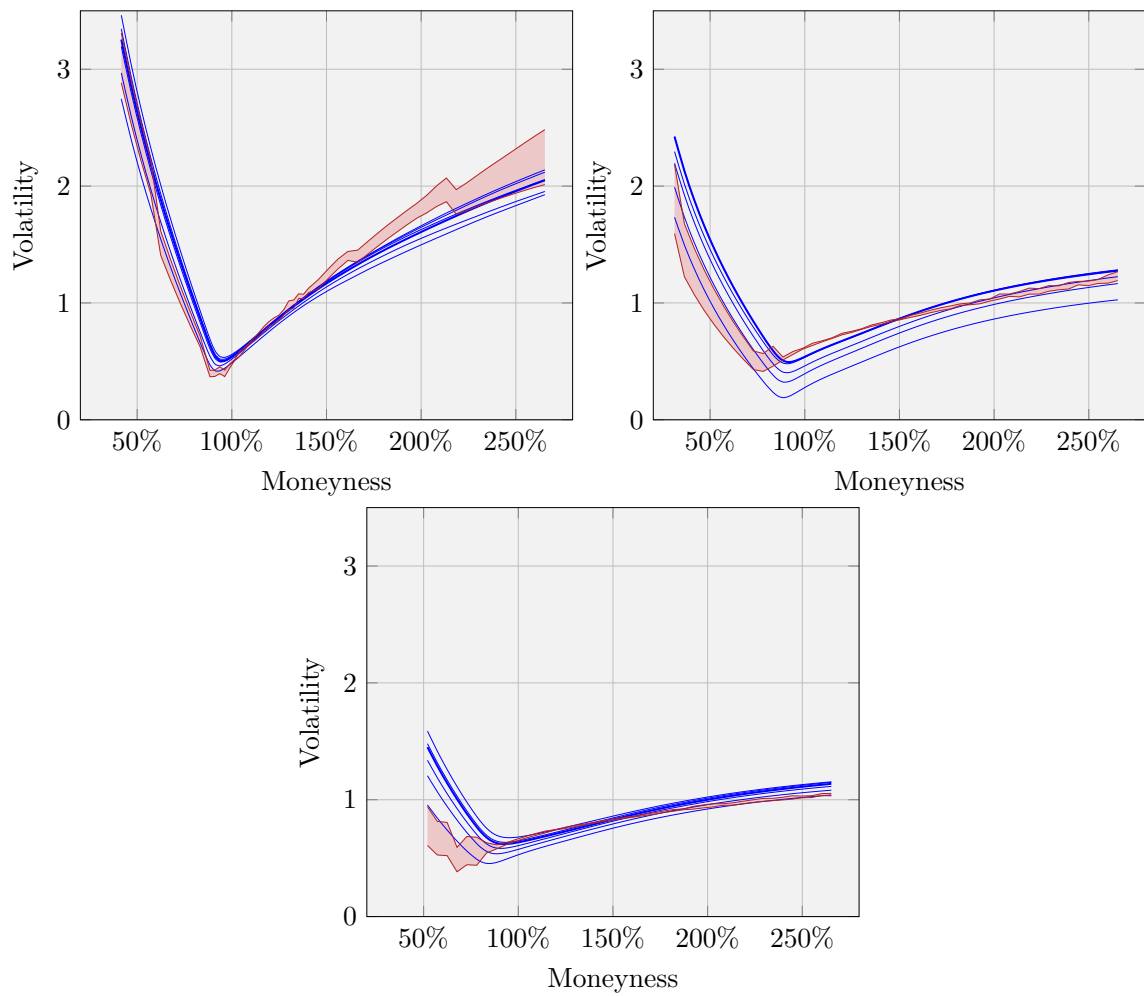


Figure 3: Impact on the VXX smile of the volatility of volatility. Market bid-ask quotes span the red shaded area, while model implied volatilities are the blue solid lines with volatility of volatility ranging from 0.1 to 1.3. The thick blue line is $\xi = 1.1$.

T^{VIX}	K	Ask	Bid	Model
November 20, 2019	14.0	1.2346	0.9477	1.0739
	14.5	1.2079	0.9793	1.0911
	15.0	1.2702	0.9793	1.1392
December 18, 2019	15.0	0.9409	0.8149	0.8642
	16.0	0.9583	0.8407	0.9030
	17.0	0.9932	0.8880	0.9170
January 22, 2020	16.0	0.7818	0.6776	0.7263
	17.0	0.8107	0.7132	0.7540
	18.0	0.8336	0.7386	0.7839
February 19, 2020	17.0	0.7478	0.6506	0.6896
	18.0	0.7555	0.6759	0.7103
	19.0	0.7881	0.6969	0.7360

Table 3: Implied volatility comparison between market quotes as on November 7, 2019, and the implied volatility obtained via our SLV models for VIX call options, for the four maturities and around ATM.

T^{VXX}	K	Ask	Bid	Model
November 15, 2019	19	0.4776	0.4428	0.4602
	19.5	0.5153	0.5019	0.5030
	20	0.5844	0.5426	0.5473
December 20, 2019	19	0.6116	0.6040	0.6050
	19.5	0.6333	0.6101	0.6154
	20	0.6549	0.6311	0.6329
January 17, 2020	19	0.6603	0.6443	0.6450
	19.5	0.6736	0.6503	0.6514
	20	0.6870	0.6723	0.6735

Table 4: Implied volatility comparison between market quotes as on November 7, 2019 and the implied volatility obtained via our SLV models for VXX call options, for the three maturities and around ATM.

the at-the-money level of the first maturity.

In the next subsection, we are going to build up a consistent framework in order to fix an admissible choice for all parameters that allows us to reproduce the market smiles of both VIX and VXX. In particular we check a posteriori that the choices of the mean-reversion speed and of the volatility of volatility are compatible with an admissible local correlation for most of the simulation paths.

5.3 Joint fit of VIX and VXX market smiles

Thanks to the analysis performed in Subsection 5.2, we are now able to pick a mix of parameters that enables us to get a good fit to both the VIX and VXX market smiles and that leads to an admissible correlation parameter $\rho(t, K) \in [-1, 1]$. That is, the model gives the proper correlation we need to put in the VIX and VXX dynamics, in order to reprice correctly the corresponding options, as described in Section 4. Let us summarize the parameters that we have fixed in order to perform the joint fit.

- The mean-reversion speed used in the joint fit is $a = 7.5$ (this value revealed to be

the optimal trade-off in order to recover the ATM implied-volatility level for the VXX options, while keeping a good fit for the VIX market).

- The volatility-of-volatility parameter is fixed as $\xi = 1.1$.
- The correlation between futures and their volatilities is fixed as $\rho^v = 0.75$.
- The remaining parameters used in the CIR-like volatility process are chosen by taking into account the non-violation of the Feller condition. In particular, we choose $\kappa = 2.5$, $\theta = 2.5$, $\bar{v} = 1$.

We have now all the ingredients to perform the joint fit of the implied volatilities of call options on VIX and VXX for different strikes and maturities around the ATM via the SLV method described previously which employs a Monte Carlo simulation with $5 \cdot 10^5$ paths. In Table 3 (resp. Table 4) we show the model implied volatilities on VIX (resp. VXX) around ATM, that are generated by the SLV model, and the market ones, with the relative errors.

In Figure 4 (resp. Figure 5) we show the whole implied volatilities for all strikes obtained by our SLV model and the market volatilities of VIX futures (resp. VXX) call options. Despite the irregular shape of the market VXX smiles, the fit is overall good and even remarkably good for the VIX smiles.

We complete the discussion of the results by showing some histograms of the distribution of the local correlation parameter $\rho(t, V_t)$, when evaluated on the VXX value simulated along each Monte Carlo path. We are able to check that for most of the paths the correlation values are within the admissible interval $[-1, 1]$, as required in Proposition 4.2. In Figure 6 we show the histograms for different times. In particular we notice that the distribution of the local correlation quickly flattens as the time elapses and it stabilizes around a mean value of 22%, with a standard deviation of 32%, and with less than the 3% of paths with a local correlation value exceeding 1. The local correlation in the simulation is capped to the maximum allowed value of 1. The satisfactory fit to VXX plain vanilla data shown in Figure 5 is an empirical evidence that we can safely use such regularization.

6 Conclusion and further developments

In this paper, we have provided a general framework for a calibration of Exchange-Traded Products (ETP) based on futures strategies. In a numerical simulation based on real data we have considered, as an example of ETP, the VXX ETN, which is a strategy on the nearest and second-nearest maturing VIX futures contracts. The main ingredient to achieve our goal was a full stochastic local-volatility model that can be calibrated on a book of options on a general ETP and its underlying futures contracts in a parsimonious manner.

A parameters sensitivity analysis allowed us to fix suitable values for the model parameters in order to fit the smile of the VIX and VXX ETN, with a high level of accuracy. Our specification led to an admissible local correlation function that justifies the consistency of the whole procedure. Remarkably, we found that the stochastic component of the volatility was necessary in order to fit market quotes. In other words, a purely local volatility approach is not rich enough for calibrating both the VIX and VXX markets. The implementation of a full calibration algorithm (in order to find the optimal value of all model parameters) based on neural-network techniques, in the same spirit of [Avellaneda et al.](#)

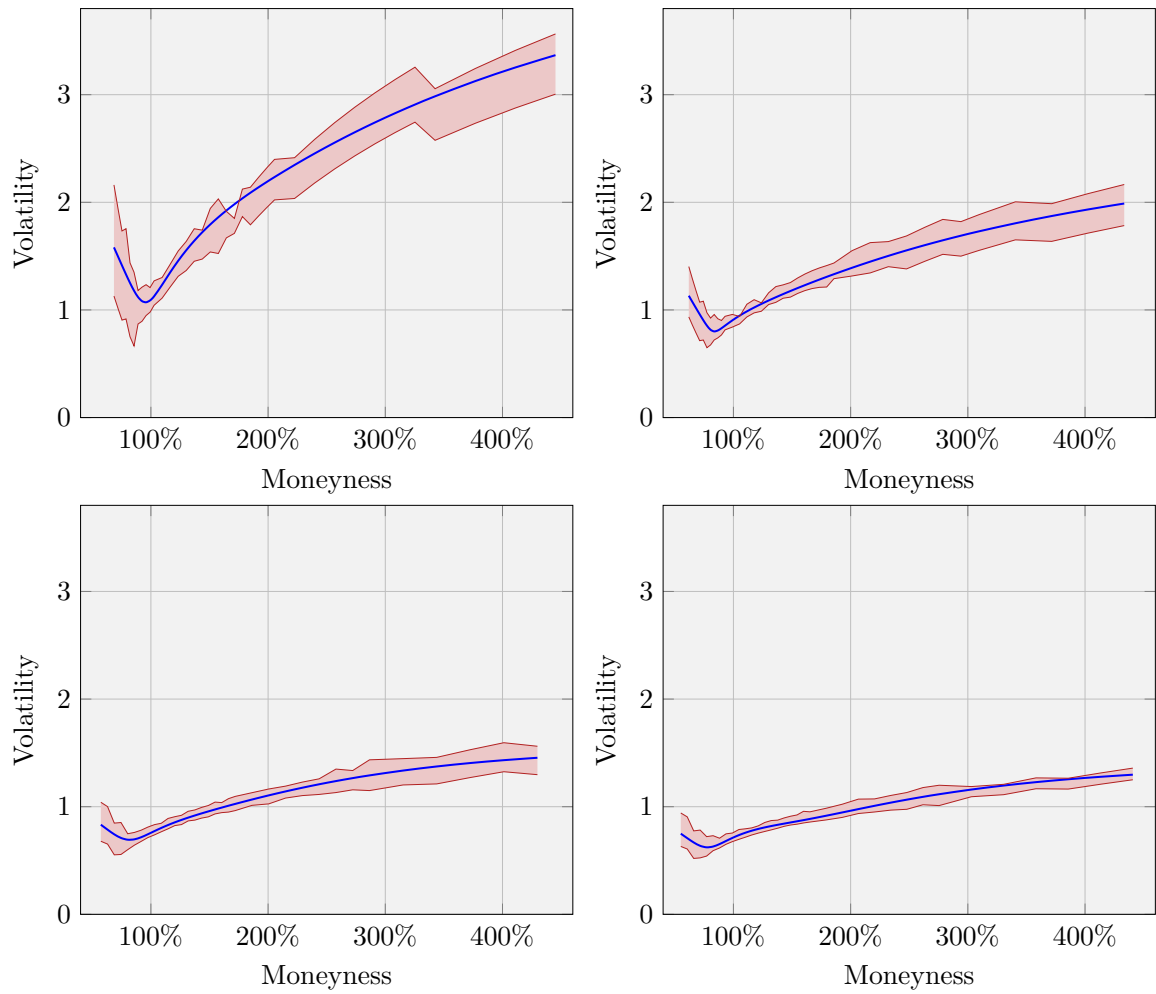


Figure 4: VIX futures model implied volatility (blue solid line) against market bid-ask quotes (red shaded area), as on November 7, 2019, for the four maturities November 20, 2019, December 18, 2019, January 22, 2020 and February 19, 2020, from the top to the bottom.

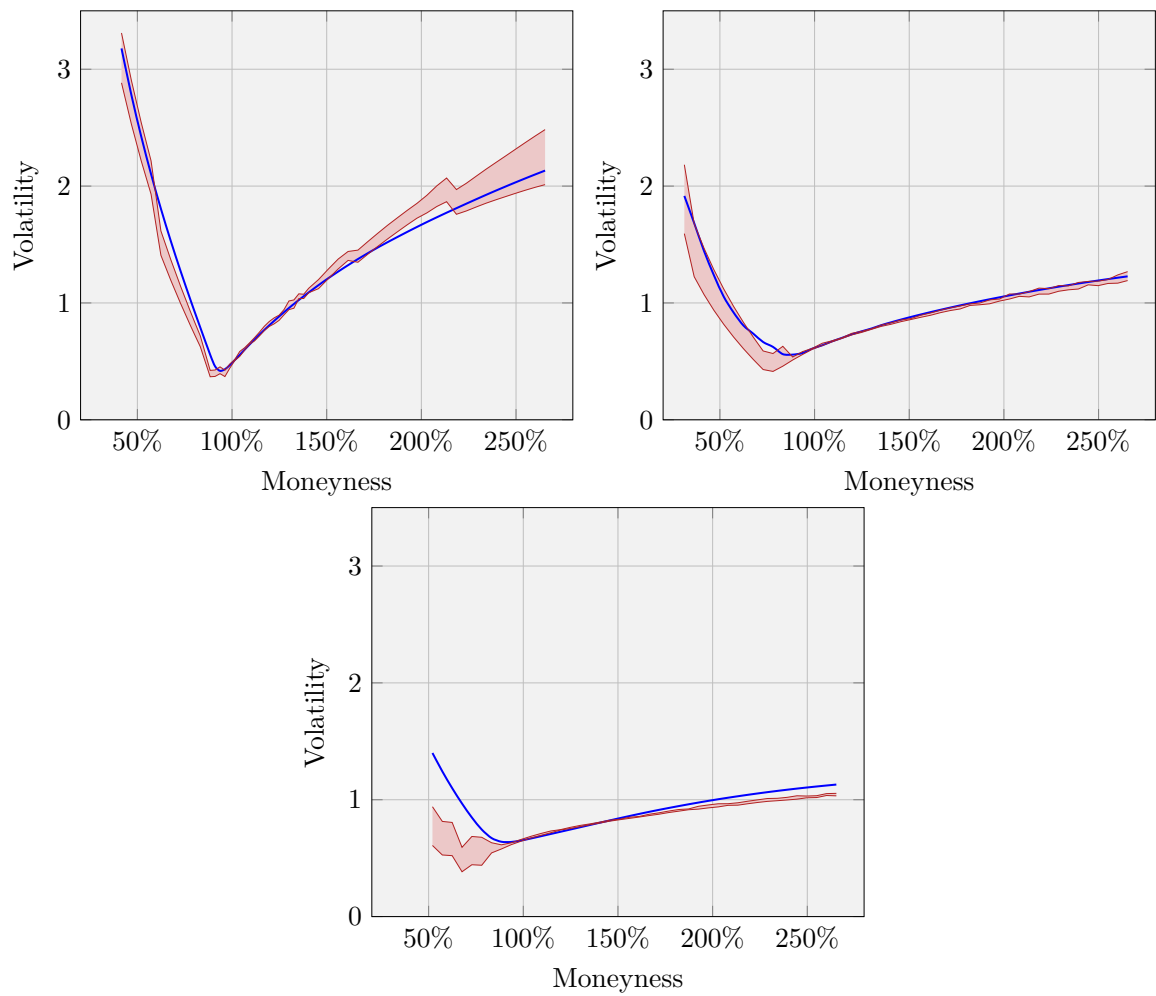


Figure 5: VXX model implied volatility (blue solid line) against market bid-ask quotes (red shaded area), as on November 7, 2019, for the three maturities November 15, 2019, December 20, 2019 and January 17, 2020, from the top to the bottom.

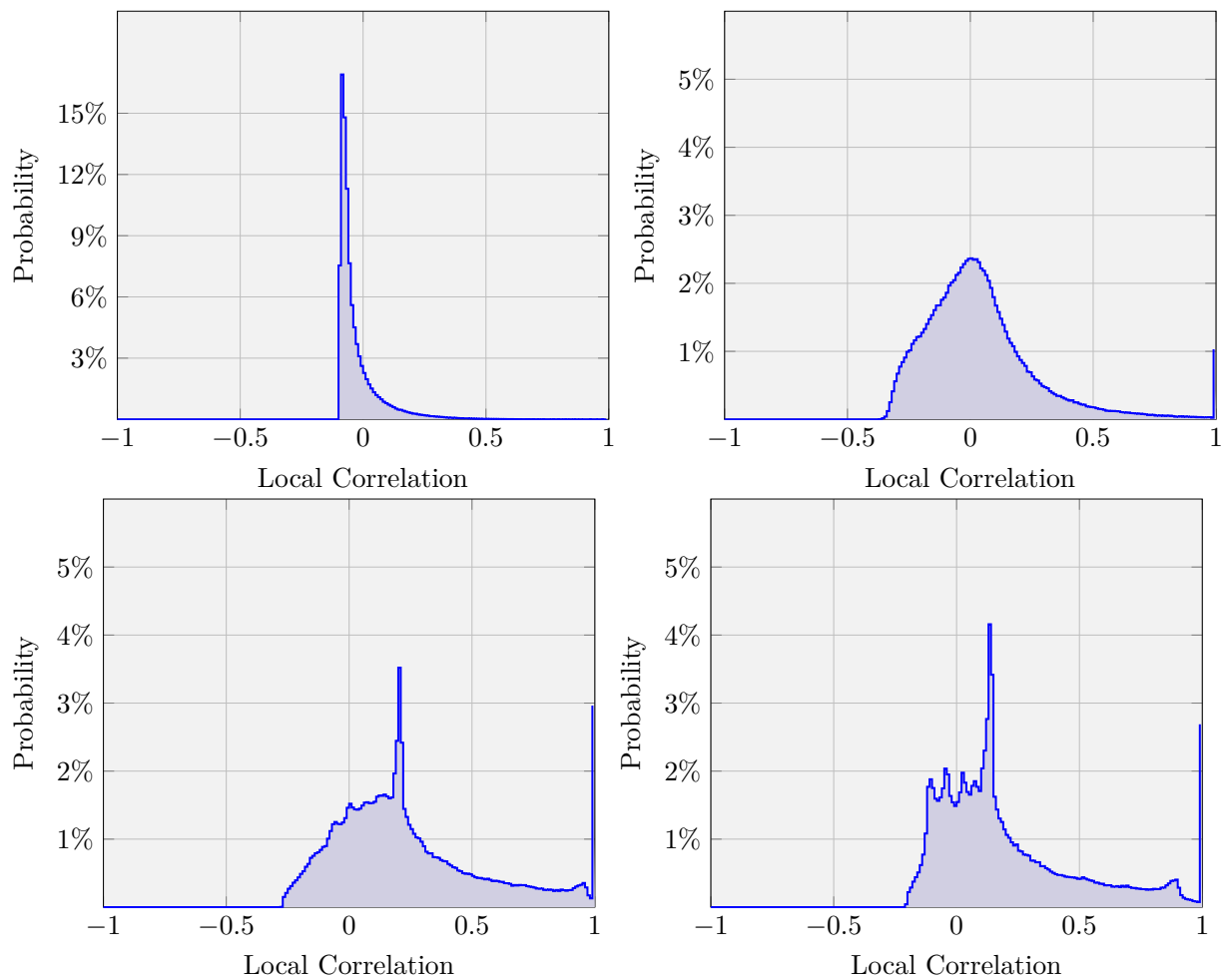


Figure 6: Histograms of the distribution of the local correlation parameter $\rho(t, V_t)$ for $t = 2, 9, 59, 67$ days.

(2021), is currently under investigation. The methodology proposed has been applied to the case of VIX futures and VXX ETN, but the framework is flexible enough to tackle also more general ETP's. Last but not least, the model is based on a simple diffusive dynamics for the VIX and it can be easily extended in order to include jumps, regime switching and other features that could be required for describing the stylized facts of this market.

References

- Alexander, C. and Korovilas, D. (2013). Volatility exchange-traded notes: curse or cure? *The Journal of Alternative Investments*, 16(2):52–70.
- Avellaneda, M., Li, T. N., Papanicolaou, A., and Wang, G. (2021). Trading signals in VIX futures. Preprint arXiv:2103.02016.
- Bao, Q., Li, S., and Gong, D. (2012). Pricing VXX option with default risk and positive volatility skew. *European Journal of Operational Research*, 223(1):246–255.
- Bergomi, L. (2015). *Stochastic volatility modeling*. CRC press.
- Cont, R. and Kokholm, T. (2013). A consistent pricing model for index options and volatility derivatives. *Mathematical Finance*, 23(2):248–274.
- Da Fonseca, J., Grasselli, M., and Tebaldi, C. (2007). Option pricing when correlations are stochastic: an analytical framework. *Review of Derivatives Research*, 10(2):151–180.
- Da Fonseca, J., Grasselli, M., and Tebaldi, C. (2008). A multifactor volatility Heston model. *Quantitative Finance*, 8(6):591–604.
- De Marco, S. and Henry-Labordère, P. (2015). Linking vanillas and VIX options: a constrained martingale optimal transport problem. *SIAM Journal on Financial Mathematics*, 6(1):1171–1194.
- Derman, E. and Kani, I. (1994). Riding on a smile. *Risk Magazine*, 7(2):32–39.
- Drimus, G. and Farkas, W. (2013). Local volatility of volatility for the VIX market. *Review of Derivatives Research*, 3(16):267–293.
- Dupire, B. (1994). Pricing with a smile. *Risk Magazine*, 7(1):18–20.
- Gatheral, J. (2011). *The volatility surface: a practitioner's guide*. John Wiley & Sons.
- Gatheral, J., Jusselin, P., and Rosenbaum, M. (2020). The quadratic rough Heston model and the joint S&P500/VIX smile calibration problem. *Risk Magazine*, 5.
- Gehricke, S. A. and Zhang, J. E. (2018). Modeling VXX. *Journal of Futures Markets*, 38(8):958–976.
- Gehricke, S. A. and Zhang, J. E. (2020). The implied volatility smirk in the VXX options market. *Applied Economics*, 52(8):769–788.
- Grasselli, M. and Wagalath, L. (2020). VIX vs VXX: A joint analytical framework. *International Journal of Theoretical and Applied Finance*, 23(5):1–39.
- Guyon, J. (2017). Calibration of local correlation models to basket smiles. *Journal of Computational Finance*, 21(1):1–51.

- Guyon, J. (2020a). Inversion of convex ordering in the VIX market. *Quantitative Finance*, 20(10):1597–1623.
- Guyon, J. (2020b). The joint S&P500/VIX smile calibration puzzle solved. *Risk Magazine*, 4.
- Guyon, J. and Henry-Labordère, P. (2012). Being particular about calibration. *Risk Magazine*, 25(1):88–93.
- Guyon, J. and Henry-Labordère, P. (2013). *Nonlinear option pricing*. CRC Press.
- Gyöngy, I. (1986). Mimicking the one-dimensional marginal distributions of processes having an Itô differential. *Probability theory and related fields*, 71(4):501–516.
- Heston, S. L. (1993). A closed-form solution for options with stochastic volatility with applications to bond and currency options. *The review of financial studies*, 6(2):327–343.
- Jex, M., Henderson, R., and Wang, D. (1999). Pricing exotics under the smile. *Risk Magazine*, 12(11):72–75.
- Lin, Y.-N. (2013). VIX option pricing and CBOE VIX term structure: A new methodology for volatility derivatives valuation. *Journal of Banking & Finance*, 37(11):4432–4446.
- Lipton, A. (2002). The vol smile problem. *Risk Magazine*, 15(2):61–66.
- Moreni, N. and Pallavicini, A. (2017). Derivative pricing with collateralization and FX market dislocations. *International Journal of Theoretical and Applied Finance*, 20(6):1–27.
- Nastasi, E., Pallavicini, A., and Sartorelli, G. (2020). Smile modeling in commodity markets. *International Journal of Theoretical and Applied Finance*, 23(3):1–28.
- Pagan, A. R. and Schwert, G. W. (1990). Alternative models for conditional stock volatility. *Journal of econometrics*, 45(1–2):267–290.
- Rebonato, R. (1999). *Volatility and correlation: In the pricing of equity, FX and interest-rate options*. John Wiley & Sons.
- Ren, Y., Madan, D., and Qian Qian, M. (2007). Calibrating and pricing with embedded local volatility models. *Risk Magazine*, 20(9):138–143.
- Schwert, G. W. (1990). Stock returns and real activity: A century of evidence. *The Journal of Finance*, 45(4):1237–1257.
- Schwert, G. W. (2011). Stock volatility during the recent financial crisis. *European Financial Management*, 17(5):789–805.
- Van der Stoep, A. W., Grzelak, L. A., and Oosterlee, C. W. (2014). The Heston stochastic-local volatility model: efficient Monte Carlo simulation. *International Journal of Theoretical and Applied Finance*, 17(7):1–30.
- Whaley, R. E. (1993). Derivatives on market volatility: Hedging tools long overdue. *The journal of Derivatives*, 1(1):71–84.

A Alternative specification for futures volatilities

Here, we describe an alternative specification for the futures volatility process given by Equation (3.22) by promoting the driving scalar process to be a matrix process.

We start with a new definition of the futures dynamics, given by Equation (3.4), which allows us to introduce the matrix driving process.

$$dF_t^i = \text{Tr} \left[\nu_t^i \cdot dW_t \right],$$

where W_t is a standard Brownian motion with values in the space of $d \times d$ matrices, and the matrix volatility process ν_t^i is defined as

$$\nu_t^i \doteq \ell_F^i(t, F_t^i) \sqrt{v_t} \cdot R_i(t, V_t),$$

where the driving process v_t has values in the space of $d \times d$ positive-semidefinite symmetric matrices. while the local-correlation processes $R_i(t, V_t)$ has values in the space of $d \times d$ orthogonal matrices, so that $R_i(t, V_t) \cdot R_i^\top(t, V_t)$ is the $d \times d$ identity matrix.

We apply the Gyöngy Lemma in order to obtain the analogue of (3.23), and thanks to the fact that for any $d \times d$ matrix A, B , we have that $\text{Tr} [A \cdot dW_t] \text{Tr} [B \cdot dW_t] = \text{Tr} [A \cdot B^\top] dt$, we get

$$\ell_F^i(t, K) = \frac{\eta_F^i(t, K)}{\sqrt{\mathbb{E}_0[\text{Tr} [v_t] \mid F_t^i = K]}}.$$

On the other hand, for the ETP strategy, we obtain

$$\begin{aligned} \eta_V^2(t, K) &= \mathbb{E}_0 \left[\sum_{ij=1}^N \hat{\omega}_t^i \hat{\omega}_t^j \text{Tr} \left[\nu_t^i \cdot (\nu_t^j)^\top \right] \mid V_t = K \right], \\ &= \mathbb{E}_0 \left[\sum_{ij=1}^N \hat{\omega}_t^i \hat{\omega}_t^j \ell_F^i(t, F_t^i) \ell_F^j(t, F_t^j) \text{Tr} \left[\sqrt{v_t} \cdot R_i(t, V_t) \cdot R_j^\top(t, V_t) \cdot \sqrt{v_t} \right] \mid V_t = K \right] \\ &= \sum_{ij=1}^N \text{Tr} \left[R_i(t, K) \cdot R_j^\top(t, K) \cdot \mathbb{E}_0 \left[\hat{\omega}_t^i \hat{\omega}_t^j \ell_F^i(t, F_t^i) \ell_F^j(t, F_t^j) v_t \mid V_t = K \right] \right]. \end{aligned}$$

We now focus on the VIX/VXX case and we select a suitable definition of the local-correlation process to recover the analogue of the result in Proposition 4.2. We assume $d = N$, where N is the number of the futures contracts, and we search for a local correlation process satisfying the following constraints: $R_i(t, K) \cdot R_i^\top(t, K) = 1$ and $\text{Tr} [R_i(t, K) \cdot R_j^\top(t, K)] = \rho(t, K)$, where $\rho(t, K)$ is a scalar function of time and price. Here, we build a solution for the case $d = N = 2$. We define the local correlations matrices $R_i(t, K)$ with $i = 1, 2$ as given by

$$R_1(t, K) \doteq \begin{bmatrix} 1 & 0 \\ 0 & 1 \end{bmatrix}, \quad R_2(t, K) \doteq \begin{bmatrix} \frac{\rho(t, K)}{\sqrt{1 - \rho^2(t, K)}} & -\sqrt{1 - \rho^2(t, K)} \\ \sqrt{1 - \rho^2(t, K)} & \rho(t, K) \end{bmatrix}.$$

In this case we can recover the analogue of the result in Proposition 4.2. In fact, from

$$\begin{aligned} \eta_V^2(t, K) &= \mathbb{E}_0 \left[\left(\hat{\omega}_t^{(1)} \ell_F^{(1)}(t, F_t^{(1)}) \right)^2 \text{Tr} [v_t] + \left(\hat{\omega}_t^{(2)} \ell_F^{(2)}(t, F_t^{(2)}) \right)^2 \text{Tr} [v_t] \mid V_t = K \right] \\ &\quad + 2\mathbb{E}_0 \left[\hat{\omega}_t^{(1)} \hat{\omega}_t^{(2)} \ell_F^{(1)}(t, F_t^{(1)}) \ell_F^{(2)}(t, F_t^{(2)}) \rho(t, V_t) \text{Tr} [v_t] \mid V_t = K \right], \end{aligned}$$

we can define

$$A^{(1)}(t, K) \doteq \mathbb{E}_0 \left[\left(\hat{\omega}_t^{(1)} \ell_F^{(1)}(t, F_t^{(1)}) \right)^2 \text{Tr} [v_t] \mid V_t = K \right],$$

$$A^{(2)}(t, K) \doteq \mathbb{E}_0 \left[\left(\hat{\omega}_t^{(2)} \ell_F^{(2)}(t, F_t^{(2)}) \right)^2 \text{Tr} [v_t] \mid V_t = K \right],$$

$$A^{(12)}(t, K) \doteq \mathbb{E}_0 \left[\hat{\omega}_t^{(1)} \hat{\omega}_t^{(2)} \ell_F^{(1)}(t, F_t^{(1)}) \ell_F^{(2)}(t, F_t^{(2)}) \text{Tr} [v_t] \mid V_t = K \right],$$

and we get the analogue of (4.31), namely

$$\rho(t, K) = \frac{\eta_V^2(t, K) - A^{(1)}(t, K) - A^{(2)}(t, K)}{2A^{(12)}(t, K)}.$$

Of course, a matrix specification for $R_i(t, V_t)$ leads to a richer (though less parsimonious) correlation structure.